



Shake-Table Experimental Testing and Performance of Topped and Untopped Cross-Laminated Timber Diaphragms

Andre R. Barbosa, A.M.ASCE¹; Leonardo G. Rodrigues²; Arijit Sinha, A.M.ASCE³; Christopher Higgins, M.ASCE⁴; Reid B. Zimmerman, M.ASCE⁵; Scott Breneman, M.ASCE⁶; Shiling Pei, M.ASCE⁷; John W. van de Lindt, F.ASCE⁸; Jeffrey Berman, A.M.ASCE⁹; and Eric McDonnell¹⁰

Abstract: This paper presents the behavior of floor diaphragms of a shake-table experiment of a full-scale 2-story mass-timber building structure. The structure consists of glued-laminated timber beams and columns, and floors and walls were designed and built making use of cross-laminated timber panels. Two different floor systems were designed, where the roof consists of a topped cross-laminated timber (CLT)-concrete composite system, and the floor level consists of untopped CLT panels connected with plywood single-surface splines. The CLT floor systems were designed to remain essentially elastic over the whole series of shake-table tests, which included testing of three lateral force-resisting systems tested at three different seismic intensity levels (service level, design basis, and maximum considered earthquake) for a total of 34 shake-table earthquake tests. Results from the testing indicate that CLT diaphragms designed to remain essentially elastic based on basic principles of structural mechanics and existing test data can achieve desired seismic performance objectives. In addition, sources of overstrength in certain elements of the diaphragm need to be explicitly considered for a holistic diaphragm design. DOI: 10.1061/(ASCE) ST.1943-541X.0002914. © 2021 American Society of Civil Engineers.

Author keywords: Cross-laminated timber (CLT); Cross-laminated timber-concrete composite floor; Diaphragm design; Resilience; Shake-table test.

Introduction

The use of cross-laminated timber (CLT) in building design and construction has increased over the last decades due to its various advantages including construction efficiency, low environmental impact, and aesthetics (Pei et al. 2016; Harte 2017). In terms of structural performance assessment and design, the most relevant research efforts in Europe and North America have focused on the performance and design of vertical elements (Ceccotti et al. 2006; Dujic et al. 2010; Popovski et al. 2010; van de Lindt et al. 2010; Ceccotti et al. 2013; Iqbal et al. 2015; van de Lindt et al. 2016; Sustersic et al. 2016; Ganey et al. 2017; Zimmerman and McDonnell 2018), which are part of lateral force-resisting systems (LFRS). Floor slabs and other horizontal elements carry the gravity

loads and constitute a majority of inertial forces. These horizontal members, under lateral loading, are designated as diaphragms and constitute an integral part of the LFRS because they are the means in which inertial forces or other horizontal forces are transferred to the vertical elements. Limited research has been conducted on the performance of CLT diaphragms and is summarized subsequently.

The behavior of CLT diaphragms is influenced by the strength, ductility, and stiffness of connections between the CLT panels and other components (Breneman et al. 2016). Floor diaphragm panels

are generally much stiffer than the corresponding connections under the in-plane loading (e.g., in-plane shear) associated with diaphragm behavior. Therefore, focus is often placed on the performance of panel-to-panel connectors. Recent works such as those by Brandner et al. (2017) have provided a good overview and an initial

¹Associate Professor, School of Civil and Construction Engineering, Oregon State Univ., Corvallis, OR 97331 (corresponding author). ORCID: https://orcid.org/0000-0003-4547-531X. Email: andre.barbosa@oregonstate.edu

²Postdoctoral Researcher, Dept. of Civil Engineering, Institute of Science and Innovation Institute for Sustainability and Innovation in Structural Engineering, Univ. of Minho, Azurém, Guimarães 4800-058, Portugal. ORCID: https://orcid.org/0000-0001-9378-1050. Email: leonardofgrodrigues@gmail.com

³Associate Professor, Dept. of Wood Science and Engineering, Oregon State Univ., Corvallis, OR 97331. ORCID: https://orcid.org/0000-0003-3718-5910. Email: Arijit.Sinha@oregonstate.edu

Note. This manuscript was submitted on October 11, 2019; approved on September 14, 2020; published online on January 21, 2021. Discussion period open until June 21, 2021; separate discussions must be submitted for individual papers. This paper is part of the *Journal of Structural Engineering*, © ASCE, ISSN 0733-9445.

⁴Cecil and Sally Drinkward Professor, School of Civil and Construction Engineering, Oregon State Univ., Corvallis, OR 97331. Email: Chris .Higgins@oregonstate.edu

⁵Technical Director, KPFF Consulting Engineers, 111 SW 5th Ave., Suite 2600, Portland, OR 97204. Email: Reid.Zimmerman@kpff.com

⁶Senior Technical Director, WoodWorks-Wood Products Council, P.O. Box D, Deer Park, WA 99006. Email: scott.breneman@woodworks.org

⁷Associate Professor, Dept. of Civil and Environmental Engineering, Colorado School of Mines, 1500 Illinois St., Golden, CO 80401. Email: spei@mines.edu

⁸Professor, Dept. of Civil and Environmental Engineering, Colorado State Univ., Fort Collins, CO 80523. Email: jwv@engr.colostate.edu

⁹Professor, Dept. of Civil and Environmental Engineering, Univ. of Washington, 214D More Hall, Seattle, WA 98195. ORCID: https://orcid.org/0000-0003-4121-0680. Email: jwberman@uw.edu

¹⁰Principal, Holmes Structures, 555 SE MLK Blvd., Suite 602, Portland, OR 97214. Email: eric.mcdonnell@holmesstructures.com

understanding of the response of CLT panels when subjected to in-plane shear stresses. However, Brandner et al. (2017) and other works did not provide concepts and methods for the design of the connectors between adjacent CLT panels that compose CLT diaphragms.

Kode (2018) performed a single reversed-cyclic test on a CLT diaphragm in support of efforts underway to systematically identify seismic performance factors for typical CLT shear-wall systems. The diaphragm test was set up as a cantilever beam following the specifications in ASTM E455-16 (ASTM 2016), and the connected CLT panels used in that experiment were designed to exhibit ductile failures in shear. The chord members used were made from rough-sawn lumber to ensure a controlled design strength for testing. Results indicated that failure of the diaphragm occurred due to the exceedance of the shear capacity of screws used to connect CLT panels and chord members. Consequently, the failure was extended to panel-to-panel connections, comprising of nailed steel splices. Results indicated that the diaphragm did not behave in the predicted manner because it had been anticipated that the diaphragm would fail in shear in panel-to-panel connections. However, the failure occurred due to tension in the self drilling screws (SDS) connecting the chord members to the CLT panels; only after this failure did the panel-to-panel connections fail in shear. Thus, the results obtained show that it is crucial to design chord members explicitly including adequate overstrength ratios so that failure of chords do not govern the strength and deformation capacity of CLT diaphragms.

Hossain et al. (2016, 2017, 2019) conducted monotonic and cyclic in-plane shear tests of varying half-lap, surface spline, and butt joint CLT panel-to-panel connection systems with one and two shear planes. Results from these tests indicated that spline connections displayed higher failure displacements and ductility values than the half-lap and butt joint connections. Sullivan et al. (2018) conducted monotonic and cyclic in-plane shear tests on half-lap and surface spline connections using varying spacings of fully and partially threaded self-tapping screws (STS). These results confirmed the increased ductility of surface spline connections and concluded that fully threaded (FT) STS have lower expected ductility than partially threaded (PT) STS, which was attributed to the FT screws failing primarily in withdrawal due to the increased bearing surface on the connected member. Thus, when comparing PT with FT STS, Sullivan et al. (2018) concluded based on their tests that PT STS are preferred for CLT diaphragms. The aforementioned summarized tests should, however, be replicated for other types of connections allowing researchers and designers to gather more data and improve their understanding on the influence of the connections and sources of overstrength of members on the behavior of CLT diaphragms.

Due to the limited research available in the literature on the performance of CLT diaphragms, current European and North American design codes and guidelines do not provide key parameters for the assessment and design of CLT diaphragms, in particular under seismic loads. In this regard, Spickler et al. (2015) developed a white paper proposing the design of CLT diaphragms using basic design principles to be used in Canada and the US. However, it does not consider overstrength of the panel shear connections to design the chords. Determination of overstrength factors lacks full-scale test results that can be used to inform and systematically document the current and future design approaches. Based on experience of the authors, in practice, the selection of the panel-to-panel connection solution are driven by constructability and cost rather than performance alone.

The main objective of this paper is to establish a new understanding of CLT diaphragm responses during intense ground motions. A mass-timber structure shown in Fig. 1 was constructed

on the University of California San Diego (UCSD) shake table to evaluate the seismic performance of two floor systems and three interchangeable shear-wall systems. The structure was designed to consist of three phases of testing, one for each lateral force-resisting system. Two of the three shear-wall systems tested in the program set resilient performance expectations, whereas the third sought to establish code-minimum expectations. Thus, the testing program addressed several performance tiers (Pei et al. 2014). Specific performance objectives for each wall system have been described by Pei et al. (2019a), Blomgren et al. (2019), and van de Lindt et al. (2019). The diaphragms were designed to remain essentially elastic throughout the testing program, setting resilient performance expectations to accommodate experimental characterization of the three shear-wall systems.

In Phase 1, a post-tensioned self-centering rocking wall design [Fig. 1(b)] was tested (Pei et al. 2019a); in Phase 2, a non-posttensioned rocking wall system, presented in Fig. 1(c), was developed and tested (Blomgren et al. 2019); and lastly, in Phase 3, a platform construction assembly, where the CLT walls were fixed through standard shear connectors and rod hold-downs [Fig. 1(d)] were tested (van de Lindt et al. 2019) as part of the FEMA P-695 project developed to propose seismic design parameters, including the R-factors estimating the ductility for the design of platform type CLT construction (Amini et al. 2018). In each of these phases, the structure was subjected to three levels of earthquake shaking: (1) service-level earthquake (SLE); (2) design basis earthquake (DBE); and (3) maximum considered earthquake (MCE). The walls were designed to carry all seismic loads transferred from the diaphragms, and the floors, beams, and columns were designed to sustain only the gravity loads. The diaphragms were designed to sustain the demands of the three different testing phases with little to no damage, or in other words, designed for the worst-case displacement and forces from all three phases.

The structure consisted of two diaphragm configurations that remained unchanged throughout the testing program of the three phases. The floor level consisted of panels connected with plywood surface splines and PT STS. The roof was a CLT-concrete composite system, in which the CLT panels were also connected between themselves using surface spline connections and the CLT panels were connected to a concrete layer using inclined screws, which allowed larger floor spans on the roof. The data collected in the testing, including accelerations measured in different locations of the diaphragms, are used to assess the influence of distinct lateral-resisting systems on the mean floor accelerations and on the transfer of inertial forces within the diaphragms. Lastly, the relative displacements measured between CLT panels as well as between CLT floor panels and glulam (GLT) beams provide valuable information regarding the stiffness and capacity of the connections designed.

Experimental Setup and Instrumentation

The dimensions of the diaphragm of the 2-story mass-timber structure tested at the UCSD outdoor shake-table are 6,096 mm (20 ft) in the east-west (E-W) direction and 17,700 mm (58 ft) in the north-south (N-S) direction. The total height of the structure above the top of the foundation is 6,700 mm (22 ft). Figs. 2(a and b) show the diaphragm plan view for the floor-level and roof-level diaphragms, respectively. The number and dimensions of the CLT panels are also shown, with a total of 16 three-ply CLT panels (nominally 104.8 mm thick) used in the floor level. Arrows on the panels indicate the major strength direction for each panel.

The roof-level diaphragm consists of a CLT-concrete composite floor system with 12 five-ply CLT panels [174.6 mm (6.875 in.)



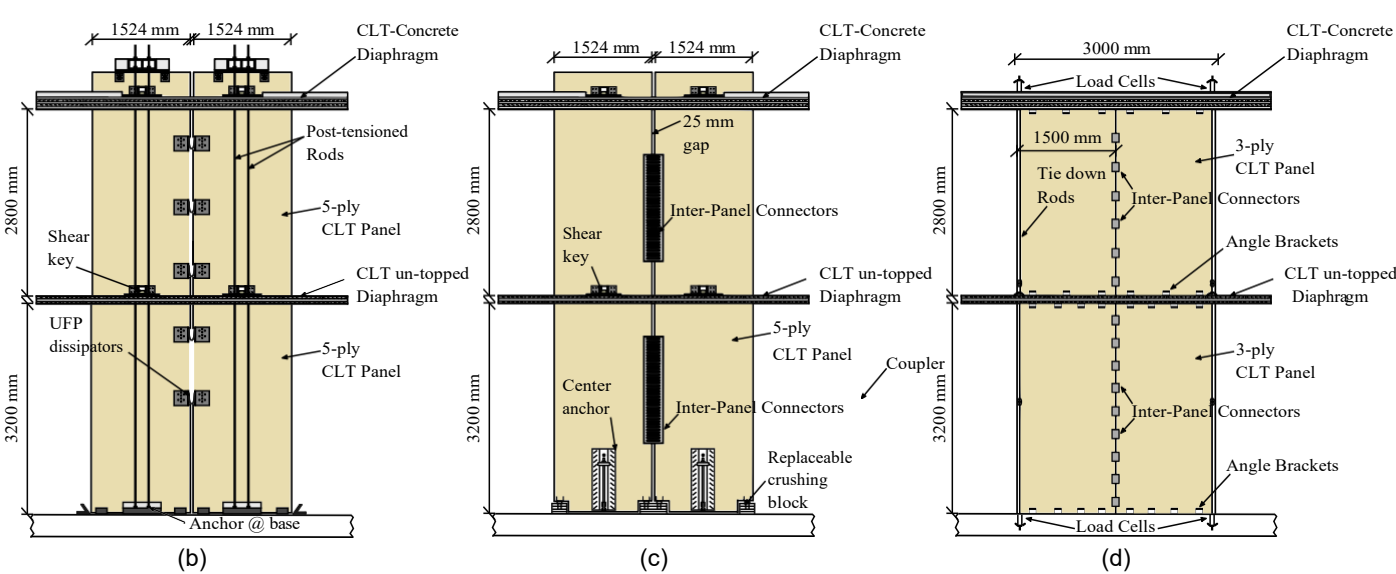


Fig. 1. Two-story mass-timber structure tested during the summer of 2017 at the UC San Diego outdoor shake table: (a) constructed structure (image by Shiling Pei); (b) post-tensioned self-centering rocking wall of Phase 1; (c) non-post-tensioned rocking wall system of Phase 2; and (d) platform construction assembly of Phase 3.

thick and a 57.2-mm (2.25-in.)-thick reinforced concrete topping slab. The CLT panels span 6,096 mm (20 ft) along the E-W direction and were connected to the concrete topping with 6.9 × 203.2 SDWH Simpson Strong-Tie SDWH27800G (Stockton, California; UES 2020) screws inclined at 45° along the span direction. The CLT diaphragm panels (DR Johnson, Riddle, Oregon) at both levels are V1 Douglas Fir grade panels (APA 2018) per ANSI/APA PRG 320 (APA 2017). The self-tapping screws used within the diaphragms are from steel grade 316, which has a minimum yield strength of 250 MPa. The surface splines constructed at both levels consisted of 19-mm-thick plywood planks fastened with PT) STS with a shank diameter equal to 5.6 mm. The cross section of the roof-level diaphragm and other design details, which are discussed in detail subsequently, are shown in Fig. 3.

The gravity load-carrying system consists of glued-laminated timber (GLT) grade L2 columns and beams from grades 24F-V4

and 24F-V8 (APA 2008). The columns located at Gridlines 3 and 5 have cross-section dimensions of 190.5 × 273.1 mm $(7.5 \times 10.75 \text{ in:})$, and remaining columns have a cross-section dimension of $190.5 \times 222.3 \text{ mm}$ (7.5 × 8.75 in:). Moreover, the columns aligned with the walls on Gridlines 3 and 5 are continuous, spanning two floors, whereas the remaining columns are interrupted at each floor level. Regarding the GLT beams placed at the floor level, two beam cross sections are defined as follows: the grade 24F-V4 beams spanning the E-W direction of the diaphragm have cross-section dimensions of 171.5 × 495.3 mm $(6.75 \times 19.5 \text{ in:})$, whereas the remaining 24F-V8 grade beams have a cross-section size of 222.3 \times 495.3 mm (7.5 \times 19.5 in:). For the roof-level diaphragm, the continuous beams between Gridlines 1 and 3a and 4a and 7 have a cross section of 222.3 × 457.2 mm $(8.75 \times 18.0 \text{ in:})$, whereas the ones located between Gridlines C and E have dimensions of 222.3 \times 381 mm (8.75 \times 15.0 in:).

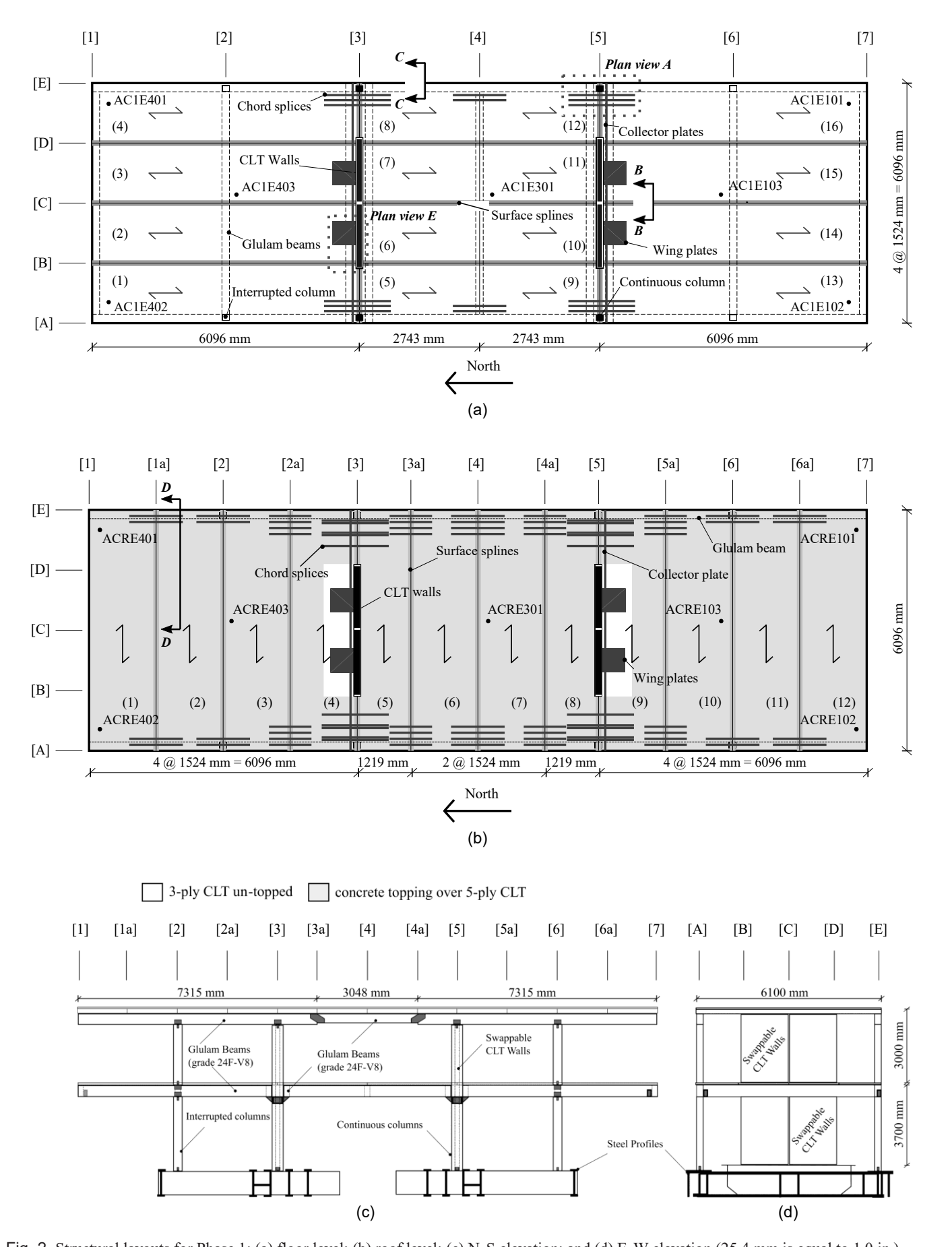


Fig. 2. Structural layouts for Phase 1: (a) floor level; (b) roof level; (c) N-S elevation; and (d) E-W elevation (25.4 mm is equal to 1.0 in.).

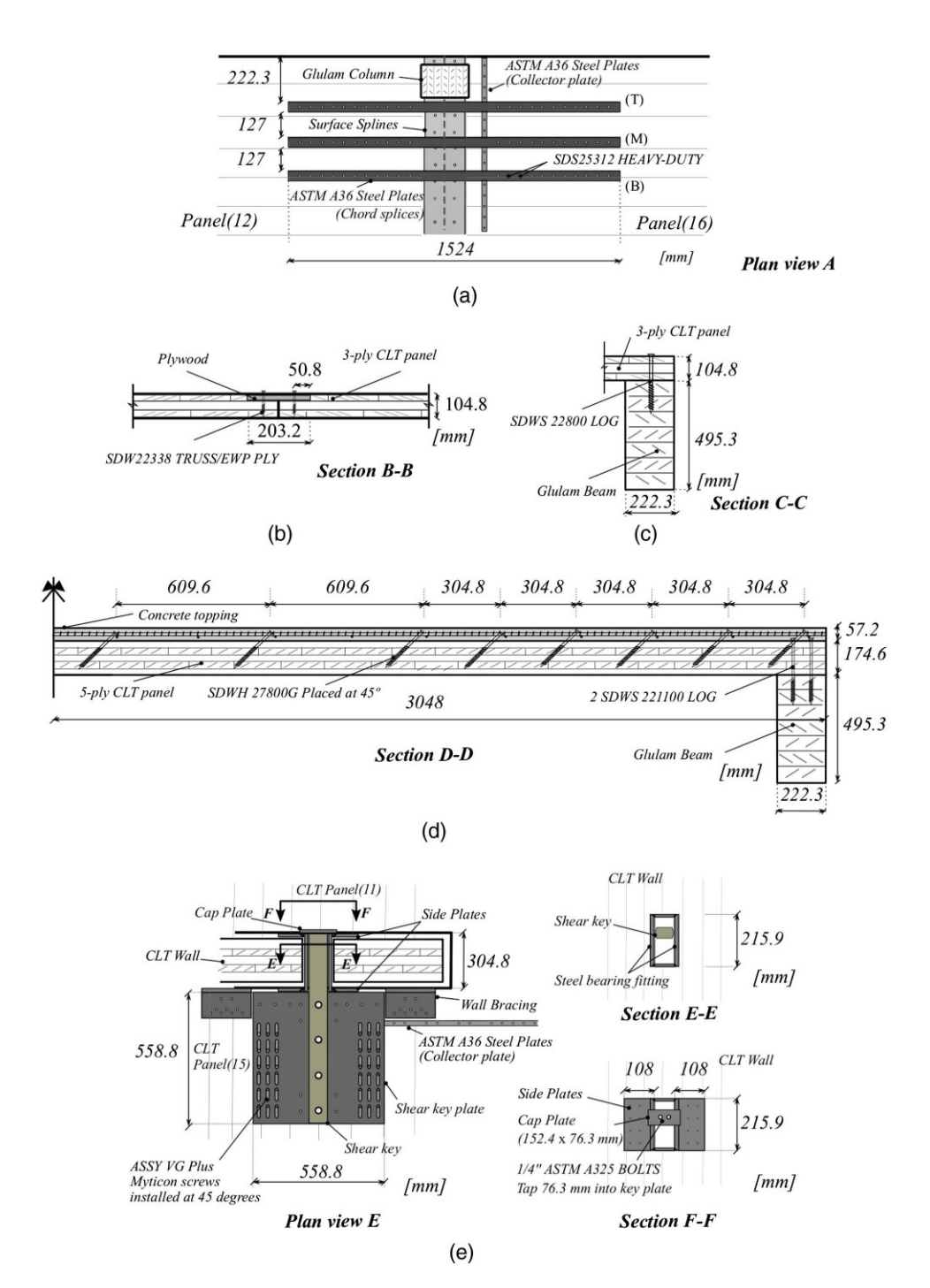


Fig. 3. Diaphragm details: (a) chord splices at the first floor; (b) single-surface spline; (c) panel connection at first floor boundaries; (d) composite diaphragm solution at the roof; and (e) shear key connection (25.4 mm is equal to 1.0 in.).

The CLT panels are connected to the GLT beams using 5.6 × 200 SDWS Simpson Strong-Tie (SDWS22800 LOG) screws and 5.6 × 279.4 SDWS Simpson Strong-Tie (SDWS221100 LOG) at the floor-level and roof-level diaphragms, respectively.

For Phases 1 and 2 (Pei et al. 2019a; Blomgren et al. 2019), when CLT rocking wall panels were used, the connection between the wall elements and the CLT diaphragms were executed through an innovative system consisting of steel shear keys. These steel shear keys were restrained to the diaphragm and slotted into the walls in order to transfer the diaphragm in-plane loads to the walls. The shear keys were free to move vertically in steel slots created in the CLT wall panels, as presented in Fig. 3(e). At the roof-level diaphragm, the shear key dimensions used were 44.5 × 76.2 mm

 $(1.75 \times 3.0 \text{ in:})$, whereas the ones placed at the floor-level diaphragm had a cross-section of only $22.23 \times 76.2 \text{ mm}$ (5=6 × 3.0 in:).

At both the floor-level and roof-level CLT diaphragms, 19-mm (3=4-in:)-thick steel transfer plates (shear key plates) were used to fix the shear keys by fastening ASTM F3125 Grade A490 bolts (ASTM 2019). As shown in Fig. 2, the shear key plates were only placed on one of the sides of the walls, which correspond to the left side of Gridline 3 and to the right side of Gridline 5, respectively.

The steel plates were fastened to the diaphragms using 10×140 ASSY VG Plus MTC Solutions (Surrey, Canada) screws installed at 45°. Moreover, complete joint penetration (CJP) welds were executed in situ to transmit the diaphragm forces from the collector plates to the shear transfer plates. Besides the steel shear transfer

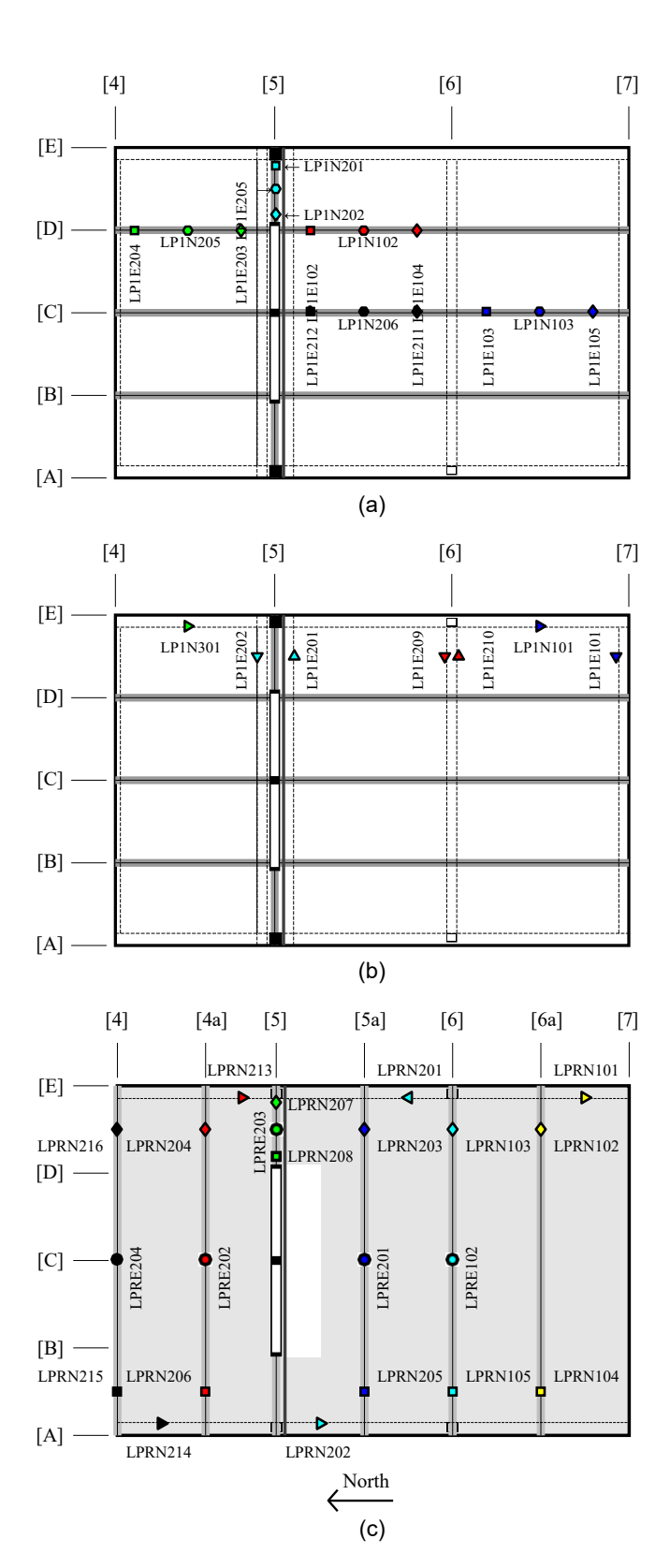


Fig. 4. Linear potentiometers placed in diaphragms to evaluate (a) surface splines at the floor level; (b) CLT-GLT beam slip at the floor level; and (c) surface splines and CLT-GLT beam slip at the roof level.

plates shown in Fig. 2, steel chords were designed and constructed on both floor levels, which remained attached to the CLT diaphragms throughout all testing phases.

In Phase 3 (van de Lindt et al. 2019), the CLT wall panels were framed in platform style. Their position was moved 609.6 mm (2 ft)

outward from the center of the diaphragms, reducing the diaphragm cantilever lengths. The test program of Phase 3 included three subphases with different wall configurations, reflecting different wall panel aspect ratios and the existence of transverse CLT walls. Further details have been given by van de Lindt et al. (2019). Of interest to this work, the connections between wall panels and diaphragms were executed using 76 × 57 × 3 mm (3 × 2.25 × 0.12 in:) L-shaped angle brackets with a length of 121 mm (4.75 in.). These brackets were fastened to the diaphragms using 19-mm (3=4-in:) fully threaded ASTM F1554 Grade 36 bolts (ASTM 2007).

Diaphragm Instrumentation

To capture the response of the CLT diaphragms, string potentiometers, accelerometers, linear potentiometers, and strain gauges were installed on the diaphragms. The string potentiometers (SP) measured absolute displacements relative to a fixed reference system, as well as vertical and in-plane displacements at distinct locations. A total of 22 string potentiometers were installed (11 at each floor). The absolute accelerations were measured using 48 uniaxial accelerometers, in which six locations measured accelerations in two horizontal directions, and eight other locations measured accelerations in three orthogonal directions. Both floors had accelerometers located at each corner as well as at quarter points along the centerline of the diaphragm, as shown in Figs. 2(a and b).

Linear potentiometers (LP) were placed to measure relative slip and separation between adjacent CLT panels as well as the slip of boundary panels over the supporting beams, but only on the south half of the diaphragms. At the roof level, LPs were also placed to measure relative displacements between CLT panels and the concrete topping. A total of 25 LPs were installed on the floor-level diaphragm, and 38 LPs were placed on the roof-level diaphragm, as shown in Fig. 4; these were installed only on the south side of the diaphragm. Sensor labels have digits and letters providing information on the location and direction of measurements. For example, reading from left to right for Sensor LP1E103, LP stands for linear potentiometer, 1 refers to the floor level, E refers to a measurement in the east-west direction, and 103 is the number of the linear potentiometer. Sensors with the letter N refer to measurements in the northsouth direction. The behavior of chord splices was monitored through 40 strain gauges placed at different locations on the chord splices.

Diaphragm Seismic Design

This section focuses on the seismic design of the diaphragms. The design of the gravity system and lateral force-resisting systems tested in the three phases have been summarized elsewhere (Pei et al. 2019a; Blomgren et al. 2019; van de Lindt et al. 2019). Both diaphragms were designed in accordance with basic principles of mechanics using values for fastener properties and member strength extracted from the most recent test results (Closen 2017; S. Pryor, personal communication, 2017) available in the literature at the time of the design, National Design Specification (NDS) from the American Wood Council (AWC 2015), and CLT manufacturer specifications (APA 2018). The Spickler et al. (2015) white paper was also used as a reference. Moreover, the alternative diaphragm design force level method described by Ghosh (2016), and included in ASCE (2016) Section 12.10.3 was used to compute the floor horizontal accelerations along the structure height. The maximum design forces were obtained for the lateral force-resisting system of the third phase that was designed for a site located in Berkeley, California (van de Lindt et al. 2019).

The respective mapped short period spectral response acceleration parameter (S_s) was equal to 2.16, which corresponds to a design spectral response acceleration parameter at short periods (S_{DS}) equal to 1.44, as defined in Section 11.4.4 of ASCE (2016). Using the formulas available from Ghosh (2016), one can see that the first mode effect is reduced by an R-factor equal to 4, which was considered for the lateral resisting system of Phase 3. However, according to Ghosh (2016), the overstrength of vertical elements generates larger first-mode forces in diaphragms. Thus, the first-mode effect is then amplified by the overstrength Ω_0 equal to 3, which is the overstrength factor used for the design of Phase 3 (van de Lindt et al. 2019).

The reduction factor R_s used to compute the diaphragm design forces was taken equal to 1.0, which corresponds to developing an essentially elastic design. The modal contribution modifier z_s considered was equal to 1.0 [Table 2 of Ghosh (2016)], and the importance factor I_e was considered equal to 1.0. Thus, the floor level was designed for an earthquake-induced horizontal acceleration equal to 1.01g, and the roof-level diaphragm was designed for 1.36g. The seismic weight assumed were 3 kN=m² (64 psf) and 3.8 kN=m² (79 psf) at the floor level and roof level, respectively.

During the design phase, the floor-level diaphragm was assumed to behave as a deep beam that responds to the in-plane loading using only the CLT properties and neglecting flexibility due to panel-to-panel connections. Consequently, the quantity of screws and their spacing at each surface spline were determined according to the shear flow caused by the inertial forces. These forces were calculated with the seismic mass and the design values for the floor accelerations, in which uniform accelerations were assumed. The chord forces were obtained through equilibrium in order to resist the diaphragm moments. These forces were divided by the number of steel plates $[6.35 \times 50.8 \text{ mm} (0.25 \times 2 \text{ in:})]$ assumed for each chord, shown in Fig. 3(a). The fasteners used in surface splines and panel-to-beam connections presented in Figs. 3(a and b) were not used to meet the requirements for continuity of diaphragm tension chords; thus, surface spline capacities were conservatively neglected in the design of the tension chords.

The CLT-concrete composite floor solution applied to the roof level was first studied by Higgins et al. (2017) for gravity loading. For the in-plane seismic design of the diaphragm, the inclined screws were designed comparing their strength (S. Pryor, personal communication, 2017) with the inertial forces computed using the floor accelerations and the concrete tributary mass. At the roof level, each surface spline was designed to guarantee the transmission of the inertial forces to the walls without considering the contribution of concrete, primarily to provide a test specimen with a maximum ratio of strength between the CLT and its concrete topping to assess the maximum CLT contribution to strength across various potential designs. It is expected that the contribution of the concrete topping would be used in design in practice. In turn, the chord splices were designed with the same method used for the first-level diaphragm, thus neglecting the additional strength provided by surface splines and concrete topping. Lastly, the CLT panels applied on both diaphragms verified the criteria given in AWC (2015) for tension, compression, and bending strength.

Limitations

The shake-table motions in the experimental program were uniaxial (E-W direction) and therefore, the response of the plan symmetric structures tested were essentially two-dimensional in nature, unlike what would be expected if the structure was subjected to three-dimensional (3D) ground motions. In addition, the horizontal diaphragm excitation was decoupled from the vertical excitation

for Phases 1 and 2, but these were not decoupled during Phase 3. To understand the coupling of the rocking of the walls in Phase 3 with the vertical motion of the floors, additional research would be required to validate future designs and modeling that captures 3D (kinematic) effects of the floor response.

Shaking-Table Test Results

A set of four historical earthquake ground motion records were scaled to fulfill the characteristics of the three design levels of shaking considered (SLE, DBE, and MCE). The records used were Northridge, 1994 (NR); Superstition Hill, 1987 (SH); Imperial Valley, 1979 (IV); and Loma Prieta, 1989 (LP). The site locations considered to scale the time-history records were San Francisco (Phase 1), Seattle (Phase 2), and Berkeley (Phase 3). More details on the record scaling have been given by Pei et al. (2019a),

Table 1. Accelerations measured at different heights of the structure

Table 1. Accelerations incasured at different neights of the structure							
		Table	Floor-level	Roof-level			
		accelerations	accelerations	accelerations			
ID	Ground motion	(g)	(g)	(g)			
	Phase 1						
1	Loma Prieta ^a	0.159	0.239	0.314			
2	Loma Prieta ^a	0.177	0.273	0.360			
3	Northridgea	0.188	0.242	0.277			
	Superstition Hilla	0.132	0.233	0.243			
5	Northridge ^b	0.534	0.556	0.546			
6	(×2) Northridge ^b (1.25)	0.550	0.750	0.625			
7	Imperial Valley ^a	0.100	0.207	0.264			
8	(×2) Northridge ^b (1.25)	0.562	0.490	0.502			
9	Loma Prieta ^b	0.533	0.435	0.463			
10	Superstition Hill ^o	0.464	0.651	0.508			
11	Loma Prieta ^c	0.666	0.440	0.544			
12	Northridge ^c	0.767	0.684	0.634			
13	Superstition Hill ^c	0.670	0.821	0.678			
14	Northridge ^c (1.2)	0.882	0.746	0.709			
Phase 2							
15	Superstition Hill ^a	0.155	0.176	0.189			
16	Imperial Valley ^a	0.198	0.239	0.279			
17	Northridge ^a	0.107	0.169	0.204			
18	Loma Prieta ^a	0.140	0.138	0.209			
19	Superstition Hill ^b	0.533	0.527	0.405			
20	Imperial Valley ^b	0.465	0.324	0.363			
21	Northridge ^a	0.125	0.132	0.109			
22	Imperial Valley ^b	0.497	0.364	0.312			
23	Northridge ^b	0.447	0.421	0.321			
24	Northridge ^c	0.714	0.482	0.455			
25	Loma Prieta ^a	0.178	0.198	0.210			
26	Imperial Valley ^c (1.2)	0.886	0.614	0.485			
27	Northridge ^c (1.2)	0.831	0.656	0.503			
	Phase 3						
28	Loma Prieta ^{a, a}	0.250	0.364	0.495			
29	Loma Prieta ^{c, d}	0.630	0.988	1.387			
30	Loma Prieta ^{o, a}	0.420	0.651	1.092			
31	Loma Prieta ^{a, e}	0.240	0.360	0.463			
32	Loma Prieta ^{c, e}	0.660	1.449	1.443			
33	Loma Prieta ^{a, f}	0.261	0.355	0.469			
34	Loma Prieta ^{c, f}	0.680	1.152	1.550			

aSLE.

bDBE.

^dSubphase 3.1 platform construction.

^eSubphase 3.2 platform construction.

^fSubphase 3.3 platform construction.

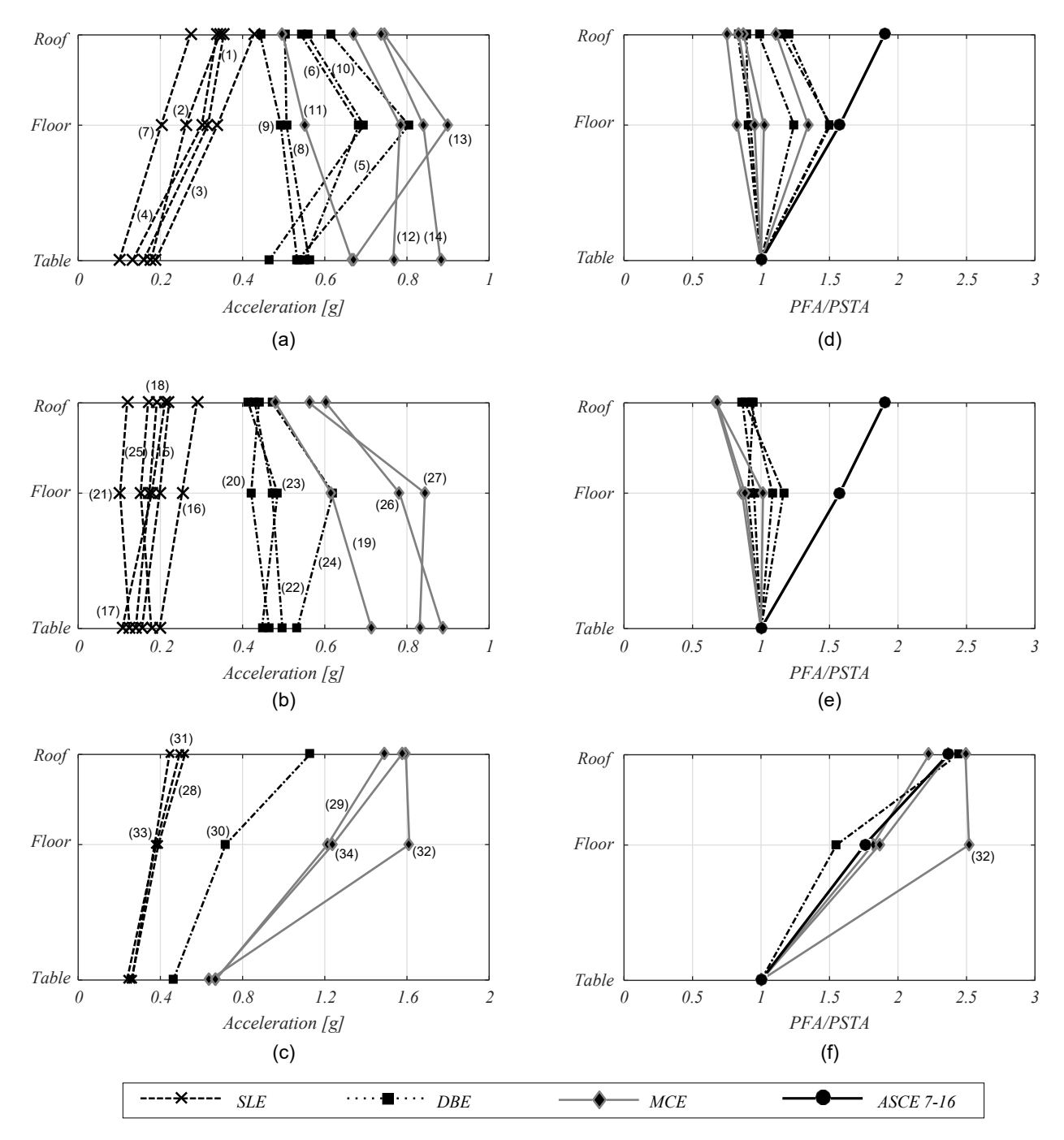


Fig. 5. Peak floor accelerations (PFA) versus structure elevation for (a) Phase 1; (b) Phase 2; and (c) Phase 3; and ratio of peak floor acceleration (PFA) to peak shake-table acceleration (PSTA) for (d) Phase 1; (e) Phase 2; and (f) Phase 3. The labels presented by numbers in parenthesis refer to the ground motions displayed in Table 1.

Blomgren et al. (2019), and van de Lindt et al. (2019), for Phases 1, 2, and 3, respectively. For reference, the ground motion records and peak ground motion acceleration measured on the shake table are listed in Table 1.

Floor Absolute Accelerations

In this section, the earthquake-induced floor horizontal accelerations measured during the 34 shaking tests are used to assess whether a general alternative diaphragm design procedure (Ghosh 2016) may apply to CLT systems. Table 1 lists the sequence of ground motions applied to the structure for all phases of testing,

where each record is assigned an identification (ID) number. In addition, the table also lists the peak ground accelerations measured at the level of the shake table. The floor absolute accelerations presented in Table 1, and also shown in Fig. 5, are the average of the peak acceleration values measured by accelerometers at the central part of the diaphragm. Thus, the reported acceleration values represent the acceleration measured at the centroid of the diaphragms and purposely exclude the measurements of the sensors placed at diaphragm corners (Fig. 2), which will be focus of another discussion subsequently. In addition, the results presented were obtained after removal of spurious spikes in the acceleration data through the use of an eighth-order low-pass Butterworth filter with a cutoff

frequency of 30 Hz (the fundamental frequency identified for Phase 1 was approximately 1.35 Hz).

Fig. 5 shows the envelope of the measured floor absolute accelerations along the height of the structure as well as the acceleration profiles used during the design process (Ghosh 2016) for each experimental phase. For both Phases 1 and 2, which correspond to

results shown in Figs. 5(a and b), it can be seen that for the SLE level of shaking, the floor accelerations (in general) increased along the height of the structure, which was expected given the mainly elastic response of the structural systems at this level of shaking. For the SLE level, the ratio of peak floor acceleration (PFA) to peak shake-table acceleration (PSTA) observed during Phase 1 for both diaphragm levels peaked at approximately 1.5 and occurred at the roof. Similar responses were observed in Phase 2, but with a lower PFA/PSTA of approximately 1.2. The difference in results for the ratios between the first phase and the second phase are related to the different vertical lateral force-resisting systems.

For Phases 1 and 2 and for the DBE and MCE levels of shaking, it can be seen that in general, the PFA/PSTA ratio tended to decrease as the intensity of the earthquake increased. This observation can be associated with the fact the CLT wall panels at the base experienced some rocking, and for larger intensities, some components of the LFRS reached the inelastic response regime. In addition, it can be observed that the floor accelerations at the floor-level diaphragm were larger than the ones measured at the roof level. This is related to the second mode responding elastically whereas first-mode effects are diminished due to rocking. At the DBE and MCE levels, it can be seen that the profiles do not match the linear acceleration profile that increased with structure height, and therefore do not match the linear acceleration envelope profiles that would be estimated when using the alternative diaphragm seismic design force level (Ghosh 2016). From the results obtained, the alternative diaphragm design method overpredicts the diaphragm loads at the upper levels, when rocking behavior is exhibited.

Regarding Phase 3, the alternative diaphragm design method proposed in ASCE 7-16 (Ghosh 2016) provides for similar profiles of the envelope of the floor accelerations across all levels of shaking, as can be seen in Fig. 5(c) for all the ground motions of Phase 3. The walls, in the platform type of arrangement of the structure developed for Phase 3, also tended to rock, although the rocking motion observed (van de Lindt et al. 2019) was less pronounced than the ones observed in Phases 1 and 2, as expected. Consequently, the first natural mode governed the response of the Phase 3 structure throughout the intensities of shaking. The ratio between peak floor acceleration and peak ground acceleration during DBE and MCE hazard levels ranged from 1.6 to 2.6, which are considerably larger than the ones observed for Phases 1 and 2. There is only one response shown for Subphase 3.2 (Test 32), which does not exhibit a linearly increasing trend along the height of the structure. In this test, the peak floor acceleration was higher at the floor level because the north wall side experienced extremely large (instantaneous) accelerations immediately after the failure, in shear, of nails connecting the walls to the floors with the angled brackets, as reported by van de Lindt et al. (2019).

Diaphragm Flexibility

Floor Accelerations

To evaluate the flexibility of both diaphragm solutions (CLT only on the floor level and CLT-concrete composite on the roof level), it is important to evaluate the accelerations at different locations within each diaphragm. Thus, from Figs. 6-8, the floor accelerations measured at different diaphragm locations are plotted for every shake-table test performed. Attention was paid to show

accelerations occurring at the same instant at different locations of the diaphragms, which also permits interpretation of torsional response observed during the uniaxial shake-table testing. The values presented at the north and south diaphragm extremities are the average of the accelerations measured at the two accelerometers located at the respective north and south alignments. The plots show first values obtained for instants where peak occurred at (1) cantilever right, (2) center of structure, and (3) cantilever left; then, out of these three instants, the one that is exhibited in the graphs is the one that had largest average acceleration.

Figs. 6(a-c) show that the responses of the floor-level diaphragm are in the form of a W and is owing to the flexibility of the diaphragm itself (i.e., the diaphragm does not behave as rigid). This acceleration pattern occurs when the accelerations measured in the center of the diaphragm are larger than the ones measured by the sensors aligned with Gridlines 2 and 6, but lower than the ones measured at the diaphragm corners near Gridlines 1 and 7. Under the same peak acceleration, the results indicate that for this diaphragm, the assumption of a uniform induced acceleration may lead to lower diaphragm bending moments and thus to nonconservative connection design. The cantilevers of the floor level experienced peak accelerations that were, in some cases, 1.5 times larger than their mean value. The shear key used to transfer the inertial loads to the CLT walls in Phase 1 [Figs. 3(e and f)] is positioned only between Gridlines 2a and 3 on the north side and between Gridlines 5 and 5a on the south part of the diaphragm (Pei et al. 2019a). Thus, the inertial forces generated at the central part of the diaphragm (between Gridlines 3 and 5) highlighting the Wshaped acceleration is in part due to the bending of the diaphragm between walls and also to the inherent load path.

The composite floor diaphragm exhibited more uniform accelerations across the diaphragm than the CLT-only one, as observed by the flatter lines in Figs. 6(d-f). This is mainly caused by the increased stiffness provided by the composite action between concrete and CLT. At this level, the acceleration measured at the cantilevers reached 1.2 to 1.3 times the mean acceleration of the floor. From the test results shown in Fig. 7 for Phase 2, for example, it can also be seen that minimal structure torsional response occurred [Fig. 7(b) Test 19, for example], but one can consider that the acceleration diagrams of the floor-level diaphragm are also Wshaped, especially for the MCE level of shaking. The results shown for Ground motions 24 and 26 represent cases where the accelerations measured at the cantilever ends are 30%-50% higher than the accelerations measured at the middle of the diaphragm. The roof-level diaphragm presented also higher acceleration at its extremities, which are more evident in the response to Ground motions 19 and 26 at the DBE and MCE levels of shaking, respectively. However, just as observed for Phase 1, the level of amplification of the acceleration at diaphragm cantilever ends are smaller (approximately 20%) than the ones observed in the CLT-only diaphragm.

From the scale of the *y*-axes in Fig. 8, it can be seen that the LFRS design solution for Phase 3 induced higher accelerations than the ones observed in Phases 1 and 2. Furthermore, due to the nature of the observed damage between different subphases for the Phase 3 testing and the effort involved to repair and replace walls (van de Lindt et al. 2019), fewer shake-table tests were possible at each intensity of shaking. For Phase 3, the floor-level diaphragm presented a W-shaped response with higher peak accelerations at the cantilevers and at the central part for the SLE level of shaking. For shaking with greater intensity (DBE and MCE), one can see that the north side (Gridline 1) exhibited higher peak accelerations, which is mainly due to the observed torsional response when the north wall connections failed. In this test, the response mode of the

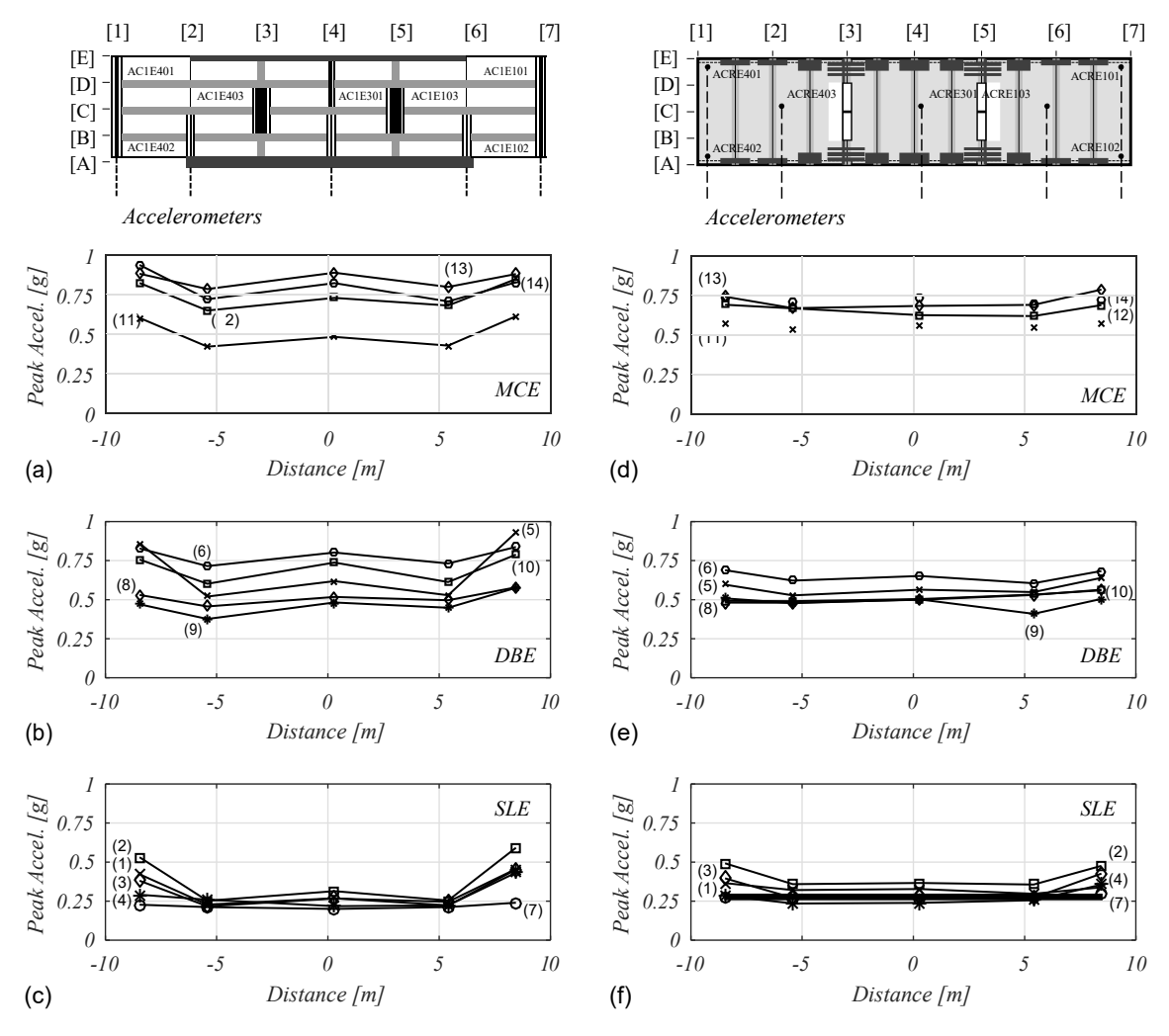


Fig. 6. Diaphragm peak accelerations measured during Phase 1 for the first floor level at (a) MCE intensity of shaking; (b) DBE intensity of shaking; (c) SLE intensity of shaking; and (f) SLE intensity of shaking. The labels presented by numbers in parenthesis refer to the ground motions displayed in Table 1.

walls shifted from predominantly rocking to sliding, with failure observed at a peak value of 56.1 mm in sliding at the base (van de Lindt et al. 2019). After Test 32, the LFRS was changed for a solution similar to the one built in Subphase 3.1 with an inclusion of transverse walls (N-S), fixed to the main CLT wall panels (E-W).

According to the results of Tests 33 and 34, shown in Figs. 8(a and c), one can conclude that even though the W-shaped response is still discernible, the effect of torsion was greatly reduced. Results in Figs. 8(d and f) indicate that the roof-level diaphragm exhibited overall a rather uniform peak acceleration profile for all the hazard levels considered. Comparing the diaphragm responses of Phase 1 and Phase 2, one can also conclude that the swap of the rocking walls, executed between these phases, had slight or negligible influence on the peak acceleration diagrams presented. The Phases 1 and 2 shear-wall systems were designed as an inverted pendulum self-centering rocking mechanism. The Phase 3 wall systems also behave in rocking, but the base connections were designed to meet standard code-minimum provisions, including ductility and economy of the design.

Diaphragm Deformations

The response of diaphragms can also be evaluated through the deformation response, especially of the connections. From the

inspections performed after each shaking-table test, it was possible to confirm that the floor-level diaphragm experienced very little damage throughout all the phases of testing, and thus an essentially elastic response was obtained as defined during the specimen design. At the roof level, there was no observation of damage on the timber panels. Nonetheless, there were minor shrinkage cracks resulting from the concrete curing process, which did not increase in size throughout the testing program; cracks were also observed along the line of the inclined screws where the nominal 19-mm (3=4-in:) cover may have been insufficient. Additionally, during the third phase of testing, small cracks were observed near the walls and in areas used in the installation of bolts. In future testing programs, due to the difference in stiffness of the timber and concrete as it cures, monitoring of dimensional changes of timber and crack growth due to the shrinkage of concrete would be of interest to increase knowledge of these effects.

Fig. 9 shows the results of measured deformations for representative linear potentiometers for the DBE and MCE levels of shaking for all three phases. In addition, for reference, the position of the linear potentiometers used to measure separation and slip are also shown. Overall, it can be first observed that the connections exhibited larger deformations during Phase 3 due to the higher intensities of its ground motions. Furthermore, even though the ground motion shaking was of larger intensity for Phase 3, the

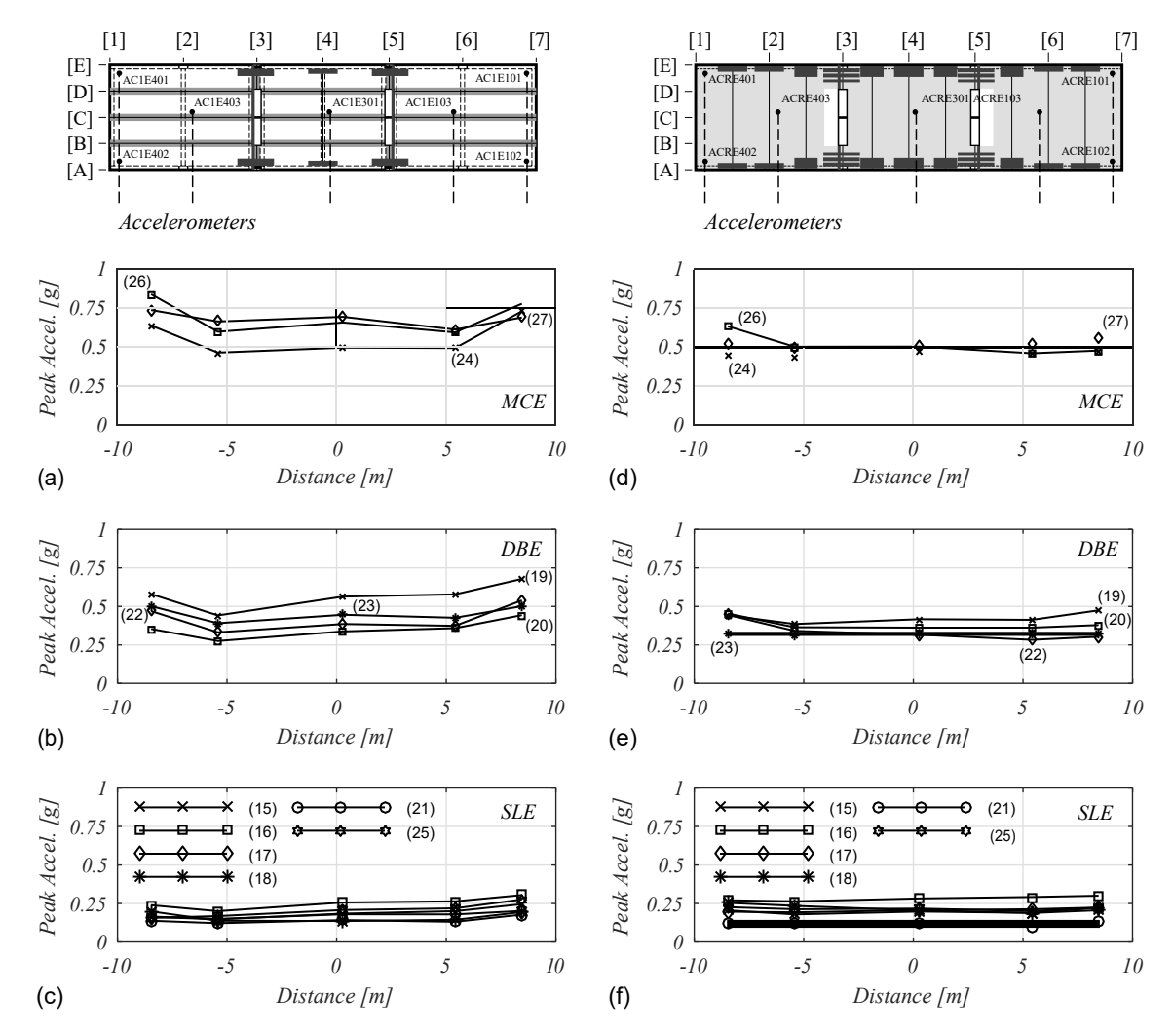


Fig. 7. Diaphragm peak accelerations measured during Phase 2 for the first floor level at (a) MCE intensity of shaking; (b) DBE intensity of shaking; (c) SLE intensity of shaking; and for the roof at (d) MCE intensity of shaking; (e) DBE intensity of shaking; and (f) SLE intensity of shaking. The labels presented by numbers in parenthesis refer to the ground motions displayed in Table 1.

amplification of ground shaking is enhanced due to the system response when compared with the other two phases. Second, more indepth analysis of the results at each floor level can be made. At the floor-level diaphragm, the surface splines oriented N-S exhibited larger values of separation [Fig. 9(a)] than slip [Fig. 9(b)]. Despite the small relative displacements measured, the assumptions made in the design process did not consider the effect of separation between panels. During Phases 1 and 2, the relative displacements measured by LP1E205 and LP1N102 were the highest values in terms of slip motions, which reached 0.4 mm (Test 13) and 0.3 mm (Test 27), respectively. These splines, along Gridline 5 between Gridlines D and E, were responsible for transmitting the inertial loads from the center of the diaphragm to the steel shear keys.

According to the design method applied for the floor-level diaphragm, the surface splines aligned with Gridline C [Fig. 2(a)] were the ones that would reach higher loads. Nonetheless, the experimental results indicate that the relative displacements (separation and slip) of surface splines along Gridline C between Gridlines 5 and 6 were negligible. On the other hand, as shown in Fig. 9(a), the separation between Panels 14 and 15 increased between Gridlines 6 and 7. This deformation can be explained by the deflection of CLT diaphragm panels, which behave like cantilevers from Gridline 5 outward toward the tip and due to a partially composite

behavior, which leads to increasing movement between panels going from Gridline 5 to the tip of the cantilever.

For Phase 3, the surface splines of the roof-level diaphragm had lower values of deformation when compared with the surface splines located at the floor level, even though the maximum accelerations of the topped diaphragm were 35%-68% higher than in the untopped diaphragm. In terms of separation between panels, the maximum values observed at the untopped diaphragm [Fig. 9(a)] are 26%-14% higher than the ones observed at the topped diaphragm [Fig. 9(e)]. Additionally, the maximum values of slip movements shown in Fig. 9(b) (untopped) are 9%-61% higher than the ones observed in Fig. 9(f) (topped).

However, the orientation of the panels also changed between the two floors with the surface splines aligned with the seismic load direction at the roof. Throughout Phases 1 and 2, the spline located along Gridline 5a experienced the highest values of panels separation [0.7 mm (0.028 in.)], as shown in Fig. 9(e). On the other hand, the spline located along Gridline 5 exhibited the highest values of slip. In Phase 3, the response changed and the separation between panels increased along Gridlines 4a and 6. Nonetheless, the surface splines along Gridlines 5 and 5a continued to be the ones with higher values of slip.

Overall, the spline slip and separation movements were limited to 1.0 and 2.5 mm, respectively. No damage was detected following

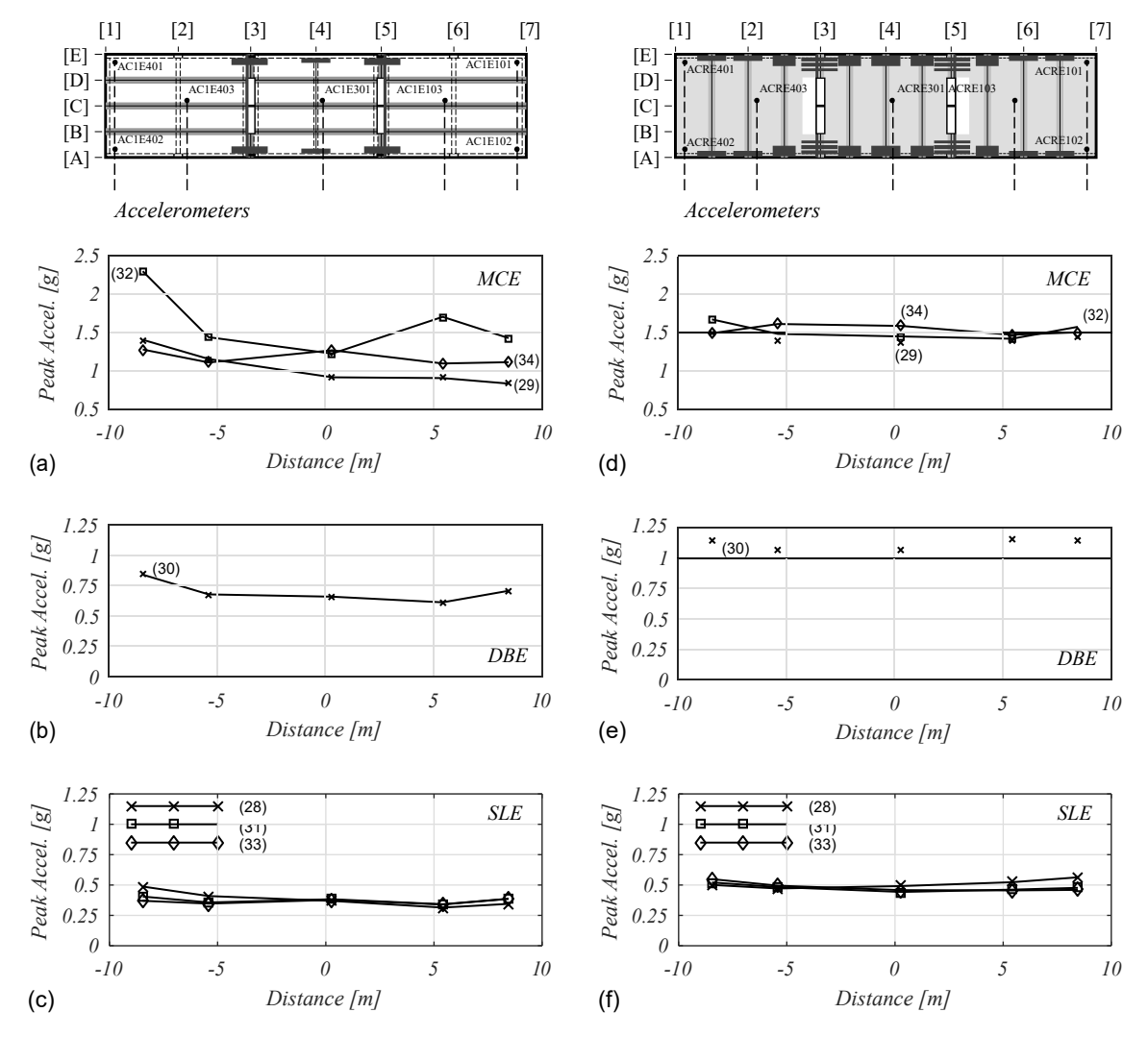


Fig. 8. Diaphragm peak accelerations measured during Phase 3 for the first floor level at (a) MCE intensity of shaking; (b) DBE intensity of shaking; (c) SLE intensity of shaking; and (f) SLE intensity of shaking. The labels presented by numbers in parenthesis refer to the ground motions displayed in Table 1.

each shake-table test. Based on this observation and supported by reference yield displacements presented by Closen (2017) and Taylor et al. (2020), in which monotonic and cyclic tests were performed on surface spline connections similar to the ones designed and built for the shake-table test, it was concluded that the spline connections of the building diaphragms exhibited an essentially linear-elastic behavior.

Lastly, even though the concrete topping presumably accounts for most of the increased rigidity, the effect of the change in the CLT thickness and span of the two floors could be further assessed in future testing and modeling of diaphragms.

Chord Splices

During the shake-table tests, measurements were also taken of the strain gauges installed on the chord steel splice plates. The chord splice described in detail here is the one that connects Panels 12 and 16 of the floor diaphragm, as shown in Fig. 3(a). Thus, it is possible to compare the forces calculated through the design approach adopted and the ones computed with the longitudinal strains measured. The approach used in the design considered the chord forces resulting from the diaphragm moments corresponding to the average peak acceleration of the roof diaphragm for the tests considered. The

fasteners used in the surface splines (located beneath the chords) were conservatively neglected in designing the diaphragm chords.

Table 2 presents the stresses (σ_s) obtained for each chord steel splice plate computed using the strain gauge measurements and assuming a Young's modulus equal to 200 GPa. The tests chosen refer to illustrate the stresses refer to DBE and MCE tests with two different ground motions, namely Northridge and Superstition Hill. As expected, the exterior plate exhibited larger stresses (larger strains were measured) due to its position.

On the other hand, the stresses (σ_a) were evaluated by computing the bending moment demand on the diaphragm based on the measured accelerations, assuming that equal stresses are developed on the tension steel plates. In this case, the inertial forces were obtained by multiplying the mass by the mean peak acceleration of the respective cantilever. One can observe from the values in the Table 2 that the exterior plate reached a larger strain-based stress (σ_s) than the acceleration-based stress (σ_a) for all except one of the reported tests (MCE Test 13). Even though not all tests are reported, similar observations were made for other shake-table tests. Thus, it can be said that the values obtained through the accelerations measured are conservative for the DBE level of shaking and that the design approach is conservative, but appropriate consideration of the sources of overstrength are needed for a holistic diaphragm design.

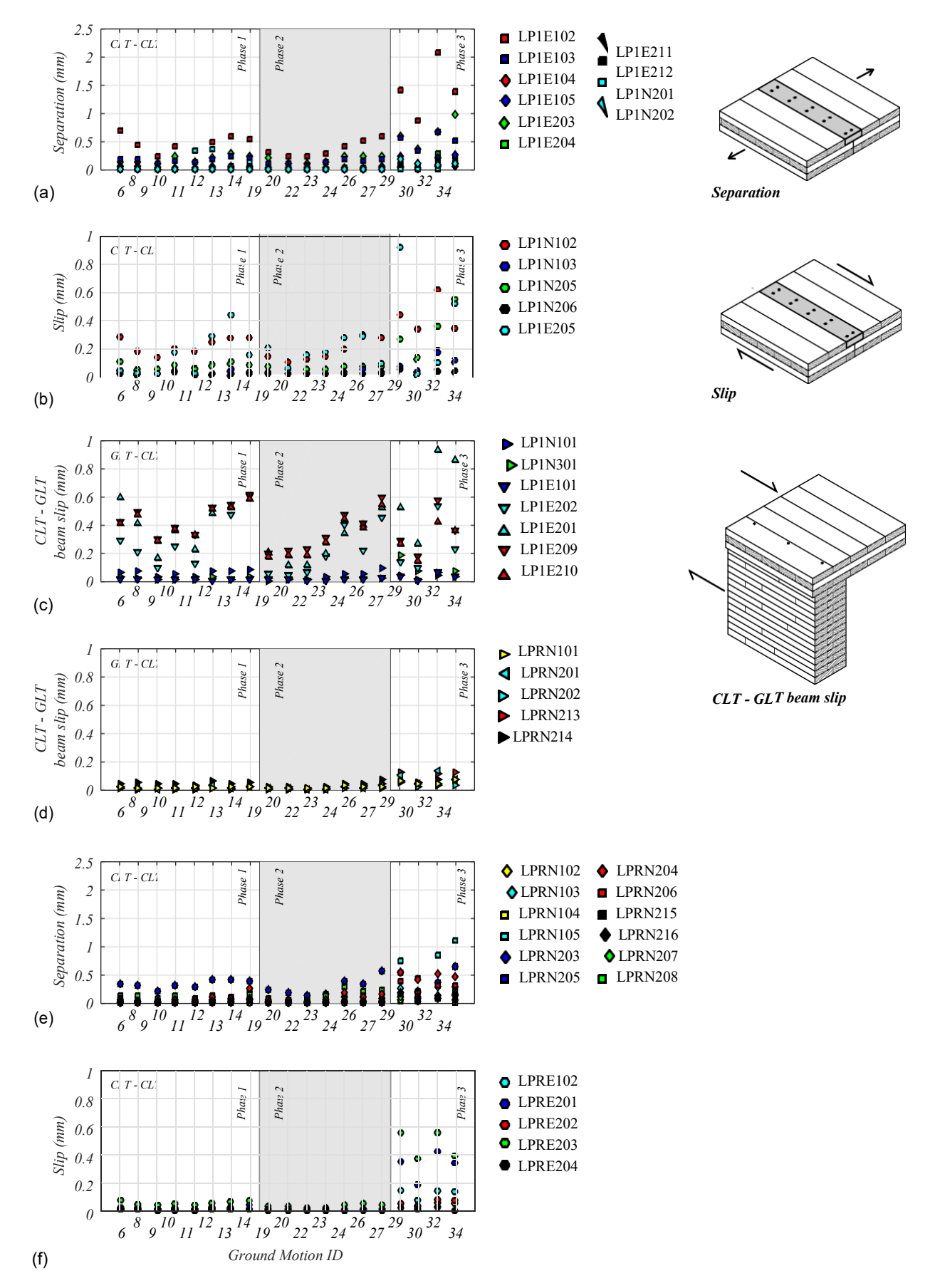


Fig. 9. Relative deformation of panel connections: (a) spline separation (floor level); (b) slip (floor level); (c) CLT-GLT beam slip (floor level); (d) CLT-GLT beam slip (roof level); (e) separation (roof level); and (f) slip (roof level) (25.4 mm is equal to 1.0 in.).

Table 2. Longitudinal stresses of chord splices at floor diaphragm

	Test	Experimental ^a		
ID	Ground motion	Plate	σ _s (MPa)	σ _a (MPa)
	_	Е	23.6	
6	(×2) Northridge (1.25)	M	19.9	44.0
_	<u> </u>	I	22.5	_
_	_	E	26.4	_
19	Superstition Hill	M	22.2	39.9
_	<u> </u>	I	17.4	_
_	_	Е	61.8	_
13	Superstition Hill	M	42.1	58.0
_	_	I	36.1	_
_	_	Е	51.4	_
14	Northridge (1.2)	M	35.5	54.1
_		I	35.1	_

Note: I = interior plate; E = external plate; M = middle plate; σ_s = strain-based stresses; and σ_a = acceleration-based stresses.

Overstrength factors should be further corroborated with component-level testing (Amini et al. 2018).

Conclusion

A 2-story full-scale mass-timber structure was tested at the UCSD Large High Performance Outdoor Shake Table, which is a Natural Hazards Engineering Research Infrastructure (NHERI) facility. Two different diaphragm solutions were designed to establish an understanding of the seismic performance of (1) a CLT diaphragm connected with surface splines, and (2) a CLT-concrete composite diaphragm. The diaphragms sustained a total of 34 shake-table tests as part of three different lateral force-resisting system solutions tested in three phases, which have been detailed in three other publications:

- Phase 1: post-tensioned rocking walls (Pei et al. 2019a);
- Phase 2: nontensioned rocking walls (Blomgren et al. 2019); and
- Phase 3: platform construction system with CLT walls connected to the diaphragms through shear anchors and rod hold-downs (van de Lindt et al. 2019).

Results indicate that the alternative design method proposed in ASCE 7-16 (Ghosh 2016) provides a reasonable distribution of accelerations along the structure height when conventional platform construction systems are used. Although conservative, it failed to predict the floor accelerations for the CLT rocking wall systems tested. Despite increases in ground motion intensity (from DBE to MCE levels), Phase-1 and Phase-2 systems limited floor accelerations because rocking lengthened the fundamental period of lateral vibrations and transmitted less force than shear walls that cantilevered more rigidly from the foundation.

The design procedure adopted in this work considered the diaphragms as deep beams where the additional flexibility due to the splines located between CLT floor panels was neglected. The inplane distribution of accelerations showed that the majority of the diaphragm response was characterized by larger accelerations at the diaphragm (cantilever) corners, whereas mainly uniform acceleration at the central core of the diaphragm was observed with minor increases of the accelerations between walls. Nonetheless, the relative displacements recorded during the shake-table tests revealed that the connections responded mainly in the elastic range as intended by the design objectives. Thus, it can be said that the design was successful given the little to no damage observed throughout all test phases. Nonetheless, smaller deformations were observed

for slip movements than for separation motions in the splines. The spline slip and separation movements were limited to 1.0 and 2.5 mm, respectively. Based on test results on splines available in the literature (Closen 2017; Taylor et al. 2020), it was concluded that the spline connections of the building diaphragms exhibited an essentially linear-elastic behavior.

The design method used did not quantify the separation between adjacent panels. These deformations can only reliably be captured through a finite-element model that explicitly includes the interpanel connection response. Additionally, the contribution of surface splines was neglected when designing the chord splices, which results in an overestimation of design chord strains and forces, which is conservative in design but should be assessed carefully to ensure ductile modes of failure of the diaphragms. Lastly, the occurrence of wall rocking at the base and between the floor and wall may induce uplift between adjacent panels at the diaphragm level, and this mode of deformation should be considered in terms of displacement compatibility in future designs, especially for platform construction.

Data Availability Statement

Some or all data, models, or code generated or used during the study are available in a repository online in accordance with funder data retention policies, including Pei et al. (2019b) or upon reasonable request to the corresponding author.

Acknowledgments

This work was financially supported by USDA Agricultural Research Service in cooperation with the Tallwood Design Institute under the Grant No. 58-0204-6-002. The second author would like to acknowledge the support of the Portuguese Science Foundation (FCT), through Ph.D. Grant No. PD/BD/113679/2015 included in InfraRisk-PhD program. The second author would also like to acknowledge the support of Oregon State University during the period in which he was a visiting Ph.D. student at this institution. Additional thanks to Simpson Strong-Tie and DR Johnson for support. This research project was also supported by the National Science Foundation through a number of collaborative awards, including CMMI 1636164, CMMI 1634204, CMMI 1635363, CMMI 1635227, CMMI 1635156, and CMMI 1634628. The use of the NHERI experimental facility is supported by the National Science Foundation's Natural Hazards Engineering Research Infrastructure (NHERI) Program. The authors would like to especially thank the NHERI at UCSD site management and staff, who helped greatly in the construction and testing program. The authors also would like to acknowledge individual industry collaborators and students who worked on this project, including Sarah Wichman, Jace Furley, Brian DeMeza, Gabriele Tamagnone, Daniel Griesenauer, Ethan Judy, Steven Kordziel, Aleesha Busch, Ali Hansan, Joycelyn Ng, Monica Y. Liu, Ata Mohseni, and Rita Barbosa. The opinions presented herein are solely those of the authors.

References

Amini, M. O., J. W. van de Lindt, D. Rammer, S. Pei, P. Line, and M. Popovski. 2018. "Systematic experimental investigation to support the development of seismic performance factors for cross laminated timber shear wall systems." *Eng. Struct.* 172 (Oct): 392-404. https://doi.org/10.1016/j.engstruct.2018.06.021.

^aStresses calculated from strains measured during experiments.

- APA (Engineered Wood Association). 2008. *Glulam product guide*. Tacoma, WA: APA.
- APA (Engineered Wood Association). 2017. Standard for performancerated cross-laminated timber. ANSI/APA PRG-320. Tacoma, WA: APA.
- APA (Engineered Wood Association). 2018. APA PR-L320 DRJ cross-laminated timber. Tacoma, WA: APA.
- ASCE. 2016. Vol. 7 of Minimum design loads for buildings and other structures. Reston, VA: ASCE.
- ASTM. 2007. Standard specification for anchor bolts, steel, 36, 55, and 105-ksi yield strength. ASTM F1554-07a. West Conshohocken, PA: ASTM.
- ASTM. 2016. Standard test method for static load testing of framed floor or roof diaphragm constructions for buildings. ASTM E455-16. West Conshohocken, PA: ASTM.
- ASTM. 2019. Standard specification for high strength structural bolts, steel and alloy steel, heat treated, 120 ksi (830 MPa) and 150 ksi (1040 MPa) minimum tensile strength, inch and metric dimensions. ASTM F3125-19e2. West Conshohocken, PA: ASTM.
- AWC (American Wood Council). 2015. National design specification for wood construction. Washington, DC: AWC.
- Blomgren, H., S. Pei, Z. Jin, J. Powers, J. Dolan, J. van de Lindt, A. Barbosa, and D. Huang. 2019. "Full-scale shake table testing of cross-laminated timber rocking shear walls with replaceable components." *J. Struct. Eng.* 145 (10): 04019115. https://doi.org/10.1061/(ASCE)ST.1943-541X.0002388.
- Brandner, R., P. Dietsch, J. Dröscher, M. Schulte-Wrede, H. Kreuzinger, and M. Sieder. 2017. "Cross laminated timber (CLT) diaphragms under shear: Test configuration, properties and design." Constr. Build. Mater. 147 (Aug): 312-327. https://doi.org/10.1016/j.conbuildmat.2017.04.153.
- Breneman, S., E. McDonnell, and R. Zimmerman. 2016. "An approach to CLT diaphragm modeling for seismic design with application to a US high-rise project." In *Proc.*, 14th WCTE World Conf. on Timber Engineering. Vienna, Austria: Vienna Univ. of Technology.
- Ceccotti, A., M. Lauriola, M. Pinna, and C. Sandhaas. 2006. "SOFIE project-cyclic tests on cross-laminated wooden panels." In Vol. 3 of *Proc.*, 9th World Conf. on Timber Engineering 2006 (WCTE 2006), 2663. Portland, OR: Oregon State Univ. Conference Services.
- Ceccotti, A., C. Sandhaas, M. Okabe, M. Yasumura, C. Minowa, and N. Kawai. 2013. "SOFIE project—3D shaking table test on a seven-storey full-scale cross-laminated timber building." *Earthquake Eng. Struct. Dyn.* 42 (13): 2003-2021. https://doi.org/10.1002/eqe.2309.
- Closen, M. 2017. "Performance of CLT connections under dynamic loading." Accessed March 24, 2020. http://www.my-ti-con.com/resources/slides-clt-connections-dyn-loading-usa.
- Dujic, B., K. Strus, R. Zarnic, and A. Ceccotti. 2010. "Prediction of dynamic response of a 7-storey massive XLam wooden building tested on a shaking table." In Vol. 4 of *Proc.*, 11th World Conf. on Timber Engineering 2010 (WCTE 2010), edited by A. Ceccotti, 3629. Trentino, Italy: Trees and Timber Institute, National Research Council.
- Ganey, R., J. Berman, T. Akbas, S. Loftus, J. D. Dolan, R. Sause, J. Ricles, S. Pei, J. W. van de Lindt, and H.-E. Blomgren. 2017. "Experimental investigation of self-centering cross-laminated timber walls." *J. Struct. Eng.* 143 (10): 04017135. https://doi.org/10.1061/(ASCE)ST.1943 -541X.0001877.
- Ghosh, S. 2016. "Alternative diaphragm seismic design force level of ASCE 7-16." *Structure Magazine*, March 1, 2016.
- Harte, A. M. 2017. "Mass timber—The emergence of a modern construction material." J. Struct. Integrity Maint. 2 (3): 121-132. https://doi.org/10.1080/24705314.2017.1354156.
- Higgins, C., A. Barbosa, and C. Blank. 2017. Structural tests of concrete composite-cross-laminated timber floors. Rep. No. 17-01. Corvallis, OR: Oregon State Univ.
- Hossain, A., R. Lakshman, and T. Tannert. 2016. "Shear connections with self-tapping-screws for cross-laminated timber panels." In *Proc.*, *World Conf. on Timber Engineering*. Vienna, Austria: Vienna Univ. of Technology.
- Hossain, A., R. Lakshman, and T. Tannert. 2017. "Cyclic performance of shear connections with self-tapping-screws for cross-laminated timber

- panels." In Vol. 14 of *Proc., 16th World Conf. on Earthquake Engineering (WCEE 2017): Resilience—The New Challenge in Earthquake Engineering*, 10559. Santiago, Chile: Chilean Association on Seismology and Earthquake Engineering.
- Hossain, A., M. Popovski, and T. Tannert. 2019. "Group effects for shear connections with self-tapping screws in CLT." J. Struct. Eng. 148 (8): 04019068. https://doi.org/10.1061/(ASCE)ST.1943-541X.0002357.
- Iqbal, A., S. Pampanin, A. Palermo, and A. H. Buchanan. 2015. "Performance and design of LVL walls coupled with UFP dissipaters." J. Earthquake Eng. 19 (3): 383-409. https://doi.org/10.1080/13632469 2014 987406.
- Kode, A. 2018. "Testing of a full-scale mass timber diaphragm." M.S. thesis, Dept. of Civil and Environmental Engineering, Colorado State Univ.
- Pei, S., J. Berman, D. Dolan, J. van de Lindt, J. Ricles, R. Sause, H.-E. Blomgren, M. Popovski, and D. Rammer. 2014. "Progress on the development of seismic resilient tall CLT buildings in the pacific northwest." In Vol. 4 of *Proc., World Conf. on Timber Engineering (WCTE 2014)*, edited by A. Salenikovich, 1-9. Red Hook, NY: Curran Associates.
- Pei, S., D. Rammer, M. Popovski, T. Williamson, P. Line, and J. W. van de Lindt. 2016. "An overview of CLT research and implementation in North America." In *Proc.*, 14th WCTE World Conf. on Timber Engineering. Vienna, Austria: Vienna Univ. of Technology.
- Pei, S., J. van de Lindt, A. Barbosa, J. Berman, E. McDonnell, J. Dolan, H. Blomgren, R. Zimmerman, D. Huang, and S. Wichman. 2019a. "Experimental seismic response of a resilient 2-story mass-timber building with post-tensioned rocking walls." *J. Struct. Eng.* 145 (11): 04019120. https://doi.org/10.1061/(ASCE)ST.1943-541X.0002382.
- Pei, S., J. van de Lindt, A. Barbosa, J. Dolan, and J. Berman. 2019b. "Shake table test of a two-story mass timber building with post-tensioned rocking walls." PRJ-1717. Natural Hazards Engineering Research Infrastructure. Accessed May 24, 2019. https://doi.org/10.17603/ds2-zcb9 -ry11.
- Popovski, M., J. Schneider, and M. Schweinsteiger. 2010. "Lateral load resistance of cross-laminated wood panels." In Vol. 4 of *Proc.*, 11th World Conf. on Timber Engineering 2010 (WCTE 2010), edited by A. Ceccotti, 3394-3403. Trentino, Italy: Trees and Timber Institute, National Research Council.
- Spickler, K., M. Closen, P. Line, and M. Pohll. 2015. "Cross laminated timber horizontal diaphragm design example." Accessed November 9, 2020. https://mtcsolutions.com/resource/clt-horizontal-diaphragm-design -example/.
- Sullivan, K., T. H. Miller, and R. Gupta. 2018. "Behavior of cross-laminated timber diaphragm panel-to-panel connections with self-tapping screws." *Eng. Struct.* 168 (Aug): 505-524. https://doi.org/10.1016/j.engstruct.2018.04.094.
- Sustersic, I., M. Fragiacomo, and B. Dujic. 2016. "Seismic analysis of cross-laminated multistory timber buildings using code-prescribed methods: Influence of panel size, connection ductility, and schematization." J. Struct. Eng. 142 (4): E4015012. https://doi.org/10.1061 /(ASCE)ST.1943-541X.0001344.
- Taylor, B., A. R. Barbosa, and A. Sinha. 2020. "Cyclic performance of in-plane shear cross-laminated timber panel-to-panel surface spline connections." *Eng. Struct.* 218 (Sep): 110726. https://doi.org/10.1016/j .engstruct.2020.110726.
- UES (Uniform Evaluation Service). 2020. Simpson strong-drive SDW22, SDWS22DB, SDWH19DB, SDWS22, SDWS19, SDWH27G, SDW16 Wood screws. Rep. No. 192. Ontario, CA: Simpson Strong-Tie.
- van de Lindt, J. W., P. Bahmani, G. Mochizuki, S. E. Pryor, M. Gershfeld, J. Tian, M. D. Symans, and D. Rammer. 2016. "Experimental seismic behavior of a full-scale four-story soft-story wood-frame building with retrofits. II: Shake table test results." *J. Struct. Eng.* 142 (4): E4014004. https://doi.org/10.1061/(ASCE)ST.1943 -541X.0001206.
- van de Lindt, J. W., J. Furley, M. O. Amini, S. Pei, G. Tamagnone, A. R. Barbosa, D. Rammer, P. Line, M. Fragiacomo, and M. Popovski. 2019. "Experimental seismic behavior of a two-story CLT platform building." *Eng. Struct.* 183 (15): 408-422. https://doi.org/10.1016/j.engstruct .2018.12.079.

van de Lindt, J. W., S. Pei, S. E. Pryor, H. Shimizu, and H. Isoda. 2010. "Experimental seismic response of a full-scale six-story light-frame wood building." *J. Struct. Eng.* 136 (10): 1262-1272. https://doi.org/10.1061/(ASCE)ST.1943-541X.0000222.

Zimmerman, R. B., and E. McDonnell. 2018. "Framework—Innovation in re-centering mass timber wall buildings." In *Proc., 11th US National Conf. on Earthquake Engineering*. Oakland, CA: Earthquake Engineering Research Institute.